ELSEVIER

Surface Science 382 (1997) L690–L695

surface science

Surface Science Letters

X-ray standing wave investigation of the surface structure of selenite anions adsorbed on calcite

Likwan Cheng [a,b], Paul F. Lyman [a], Neil C. Sturchio [b], Michael J. Bedzyk [a,c,*]

[a] *Materials Science Department and Materials Research Center, Northwestern University, Evanston, IL 60208, USA*
[b] *Environmental Research Division, Argonne National Laboratory, Argonne, IL 60439, USA*
[c] *Materials Science Division, Argonne National Laboratory, Argonne, IL 60439, USA*

Received 13 January 1997; accepted for publication 20 February 1997

Abstract

The adsorption of selenite ions (SeO_3^{2-}) from a dilute aqueous solution onto a freshly-cleaved calcite ($10\bar{1}4$) surface was studied with the X-ray standing wave (XSW) technique. The complex ion SeO_3^{2-} is found to selectively adsorb at the CO_3^{2-} site via ionic exchange, forming a two-dimensional solid-solution of the form $Ca(SeO_3)_x(CO_3)_{1-x}$ at the interface. The calcite ($10\bar{1}4$), (0006) and ($11\bar{2}0$) Bragg reflections were used to triangulate the Se position with respect to the calcite lattice. The local surface structure at the SeO_3^{2-} adsorbate site, derived from the XSW results, is consistent with a model in which the base of the SeO_3^{2-} trigonal pyramid aligns with (and replaces) the CO_3^{2-} equilateral triangular group. The SeO_3^{2-} adsorption saturated at a coverage of 0.02 monolayers. Under identical chemical conditions, selenate (SeO_4^{2-}) adsorption was inhibited. © 1997 Elsevier Science B.V.

Keywords: Adsorption; $CaCO_3$; Calcite; Low-index single crystal surfaces; Selenite; SeO_3; Surface structure; X-ray standing waves (XSW)

The interaction of dissolved trace element species with mineral surfaces is fundamental to a wide range of phenomena. It has implications for a wide range of geochemical issues, including geochronology, palaeoclimatology and biomineralization, as well as critical applications in ore mineral processing, nanoengineering technology, and in understanding the environmental transport of toxic and hazardous metals. For example, one of the principal controls on the transport of toxic metal species in groundwater aquifers is adsorption by mineral surfaces. One such metal of particular concern for human health is selenium, this is potentially hazardous to human and animal health in trace amounts.

In groundwaters, selenium is transported predominantly as the two divalent oxyanions selenite (SeO_3^{2-}), in which selenium is tetravalent, and selenate (SeO_4^{2-}), in which selenium is hexavalent [1]. These selenium ions are also taken up selectively from soil water by certain edible plants [2], thus constituting another potential pathway to human toxicity. Understanding the molecular-scale interactions of selenium ions with mineral surfaces is a prerequisite for elucidating the macroscopic redistribution of these ions in soils and groundwaters. While these interactions may involve

* Corresponding author. Fax: +1 847 4672269; e-mail: bedzyk@nwu.edu

PII S0039-6028(97)00167-2

adsorption, precipitation, dissolution and oxidation–reduction processes, the current investigation focuses on adsorption.

Adsorption of selenium ions by mineral surfaces has been studied experimentally on oxides and hydroxides [3–6], with molecular-scale information being obtained by extended X-ray absorption fine structure measurements (EXAFS) [5,6]. Most of these studies, with one exception [6], have concluded that selenite forms inner-sphere complexes with these surfaces, while selenate does not. Additionally, selenite adsorption on calcite has been studied using a powder surface isotope exchange technique employing radiochemical counting of liquids from batch experiments [8]. The results of this previous study [8] indicated that selenite adsorbs on calcite via surface ion exchange with carbonate ions, over a range of solution pH for selenite concentrations of 10^{-7} to 10^{-6}M. The coverage of selenite ions was less than 5% under all measured conditions, but no direct observations of the calcite surface were obtained to verify the location of the adsorbed selenite [8]. Trace amounts of selenate have been shown by EXAFS to be incorporated with some distortion into the carbonate site of calcite during growth [1,9].

Herein, we describe an X-ray standing wave (XSW) investigation of the adsorption of SeO_3^{2-} and SeO_4^{2-} from water onto the $(10\bar{1}4)$ cleavage surface of single crystal calcite. In the XSW technique, the combination of elemental chemical specificity and atomic-scale spatial resolution allows the direct probing of the Se atomic site with respect to the calcite lattice after adsorption. Our experiments show that SeO_3^{2-}, but not SeO_4^{2-}, adsorbs on calcite at a measurable coverage when the calcite surface is placed in contact with a 10^{-4}M Na_2SeO_3, or Na_2SeO_4, solution. For SeO_3^{2-} adsorption (see Fig. 1), the Se site on a calcite $(10\bar{1}4)$ surface was precisely determined by XSW triangulation [10] with respect to the $(10\bar{1}4)$, the (0006) and the $(11\bar{2}0)$ diffraction planes. The Se lattice position thereby determined gives information on the adsorption site of the SeO_3^{2-} ion on the calcite $(10\bar{1}4)$ surface, and hence reveals the nature of the bonds that are formed between the SeO_3^{2-} adsorbate ion and the surrounding calcite substrate lattice. The nature of this bonding, i.e. physical or chemical, offers insight into the stability of the adsorbate at the water–calcite interface, and therefore its transport behavior in the environment. This study, along with our recent XSW studies of Pb^{2+} on calcite [11,12], represent an important new approach for the atomic-scale investigation of adsorption of elemental and complex ions on single crystal mineral surfaces.

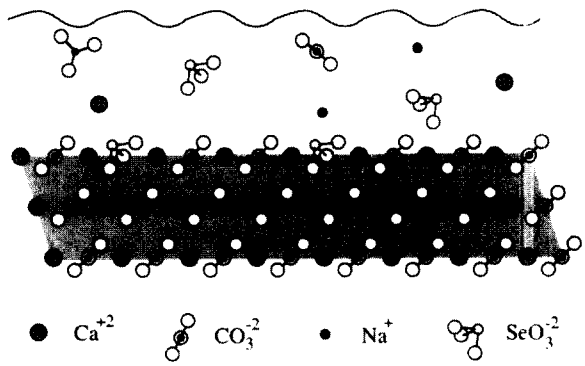

Fig. 1. A schematic representation of the interface between the Na_2SeO_3 solution and calcite $(10\bar{1}4)$ surface.

Based on the dynamical theory of X-ray diffraction from a perfect crystal [13], the interference of the coherently-coupled incident and Bragg-reflected X-ray plane waves generates an XSW in and above the crystal, with the XSW nodal planes parallel to and having the same periodicity as the diffraction planes. As the incident Bragg angle is tilted through the arc-second-wide Bragg reflection from its low-angle side to its high-angle side, the XSW undergoes a continuous phase shift of π radians. This causes an inward shift of the XSW by one-half of a d-spacing, which, in turn, causes the fluorescence yield $Y(\theta)$ of a surface adatom to exhibit a modulation that is characteristic of the adatom's location relative to the diffraction planes

$$Y(\theta) = Y_{OB}[1 + R(\theta) + 2\sqrt{R(\theta)} f_H \cos(v(\theta) - 2\pi P_H)]. \quad (1)$$

In this expression, the constant Y_{OB} is the fluorescence yield at an off-Bragg angle, $R(\theta)$ is the X-ray reflectivity, $v(\theta)$ is the relative phase of the standing wave field and $\boldsymbol{H}$ denotes the diffraction vector. The coherent position P_H is the average $\Delta d/d$

position of the adatom, and the coherent fraction f_H is related to the fraction of the impurity adatoms located at P_H. The quantities f_H and P_H are, respectively, the amplitude and phase of the Hth Fourier component of the spatial distribution of the adatoms. Experimentally, one simultaneously acquires the reflectivity R and the fluorescence yield Y while scanning in angle q through a $\boldsymbol{H}=$ *hkil* strong Bragg reflection of the substrate crystal. Eq. (1) is then fitted to the fluorescence yield to extract the values of P_H and f_H. The XSW experiments in this study were performed at the National Synchrotron Light Source, at beamline X15A. The general technique and arrangement for an XSW experiment are reviewed in Ref. [14]. Some details concerning the specific set-up at X15A have been described in Refs. [11,14,15].

SeO_3^{2-} and SeO_4^{2-} adsorption on calcite took place in aqueous solutions that were near calcite saturation and contained 100 μM of Na_2SeO_3 or Na_2SeO_4, respectively. The calcite samples were cut from large natural single crystals from Brazil, and were freshly cleaved on the $(10\bar{1}4)$ cleavage plane immediately before immersion into 4 mL of the experimental solution (pH ≈ 8) in a loosely-capped, 7-mL Teflon vial. The cleavage surface was $8 \times 8\ mm^2$. The reactions were conducted at room temperature for 3 to 11 h. After adsorption, each sample was removed from the solution (excess solution removed with a jet of nitrogen gas) and mounted on a four-circle diffractometer. The samples were maintained in an inert helium atmosphere at room temperature for the duration of the XSW measurements. Separate XSW scans were taken for the normal $(10\bar{1}4)$, and the off-normal (0006) and $(11\bar{2}0)$ reflections. The data collection times for these scans were ca. 6, 20 and 12 h, respectively. The incident X-ray beam was monochromated to an energy of 14.80 or 16.00 keV by a pair of Si(111) monochromator crystals; the first crystal had a 6°-angle miscut, thereby reducing the angular divergence of the incident beam. The reflectivity $R(\theta)$ was recorded with a Si photodiode detector, and the fluorescence spectrum was recorded by an energy-dispersive Si(Li) detector. A Mo slit placed between the sample and the Si(Li) detector restricted collection of X-rays to small emission angles to enhance the surface sensitivity of the fluorescence signal. The total Se coverage was measured by comparison to fluorescence from a standard sample calibrated by Rutherford backscattering spectrometry.

The X-ray fluorescence spectra from calcite samples after adsorption reactions in the Na_2SeO_3 and the Na_2SeO_4 solutions, respectively, were analyzed and compared to the fluorescence spectrum for an untreated calcite sample. All spectra were acquired with the same detector and slit geometry. The presence of a Se Kα peak at 11.2 keV in the fluorescence spectrum for the SeO_3^{2-}-reacted sample indicates that the SeO_3^{2-} had been adsorbed onto the sample surface. The Se Kα peak in the spectrum for the SeO_4^{2-}-reacted sample, on the other hand, was significantly weaker and insufficient for XSW analysis. XSW measurements made on the SeO_3^{2-} −reacted samples for the $(10\bar{1}4)$, (0006) and $(11\bar{2}0)$ reflections revealed that a majority of the Se atoms were located at a single preferred calcite lattice position. Representative XSW data for the reflectivity and Se fluorescence yields for angular scans through these three reflections are shown in Fig. 2, along with the theoretical fits and their respective fit parameters f_H and P_H. Also shown in Figs. 2a and b are the simulated yield curves (dashed lines) that the Se yield would have followed if Se occupied the C atomic sites.

The total Se coverage in terms of equivalent carbonate monolayers was $\Theta = 0.02 \pm 0.01$ ML (where $1\ ML = 5.04 \times 10^{14}\ atoms\ cm^{-2}$). This is comparable to the results of Cowan et al. [8]. Coverage did not change significantly as a function of reaction time (3 to 11 h), indicating that a steady state had been reached by 3 h. There was no observable decrease in the off-Bragg Se fluorescence yield throughout the XSW experiments, suggesting that Se desorption was insignificant under the experimental conditions. The coherent position values did not change over the course of time or vary with different surface preparations on different samples. The coherent fraction did, however, vary from sample to sample, indicating variances in the fraction of Se atoms which are correlated with the calcite lattice. For example, the first sample, for which the $(10\bar{1}4)$ and (0006) results are shown in Figs. 2a and b, had a $(11\bar{2}0)$

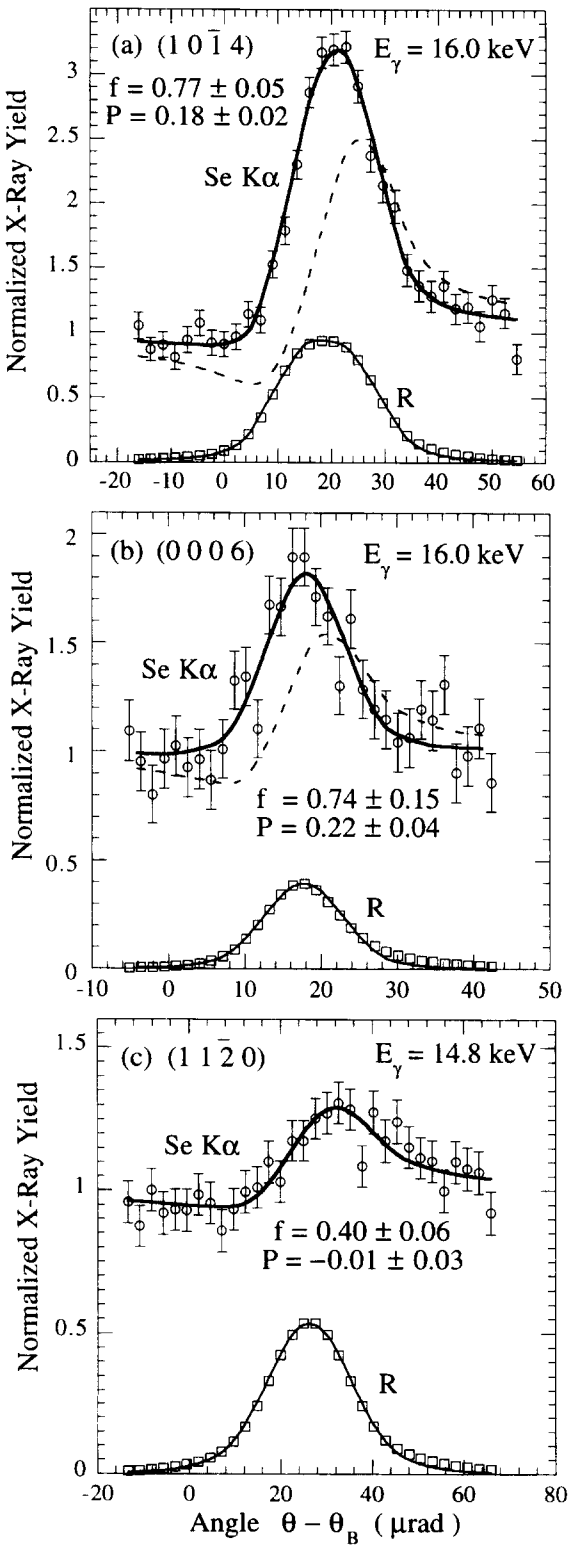

Fig. 2. The experimental and theoretical angular dependence for the X-ray reflectivity (R) and the Se Kα fluorescence yield for the calcite: (a) (10$\bar{1}$4), (b) (0006) and (c) (11$\bar{2}$0) Bragg reflections. Each theoretical yield curve (thick solid line) is based on a χ^2 fit of Eq. (1) to the Se Kα data in which the listed coherent fraction (f) and position (P) values were determined. For comparison, the dashed curves in (a) and (b) are the theoretical yield curves corresponding to the carbon site, where $P_H = 0$.

measurement (not used in this analysis due to poor counting statistics) with $f_{11\bar{2}0} = 0.75 \pm 0.27$ and $P_{11\bar{2}0} = 0.02 \pm 0.06$ in comparison to the values for the second sample which are shown in Fig. 2c. Plausible explanations for the variances in the coherent fractions are: nonuniform rinsing away of physisorbed SeO_3 and the presence of Se associated with surface contamination or step edges.

Since all three different *hkil* XSW measurements produced reasonably high values for the coherent fraction, we can safely conclude that there is only one preferred Se position with respect to the bulk calcite lattice. We will show how the measured XSW coherent positions along the three noncoplanar [*hkil*] directions are used to directly triangulate this Se lattice position. We will also show that this position agrees with a model in which the surface is unreconstructed and has 2% of the surface carbonate groups replaced through ion exchange with selenite groups. The assumption in this model places the surface Ca, C and O atoms in bulk-like positions; this is consistent with previous atomic force microscopy [16,17] and X-ray reflectivity studies [18] of the water–calcite interface which show that there is no reconstruction and no significant relaxation of the calcite surface atomic layer.

Referring to the [1$\bar{2}$10] projection of the calcite lattice model in Fig. 3a, the (10$\bar{1}$4) XSW measured position of Se is $P_{10\bar{1}4} \cdot d_{10\bar{1}4} = 0.54 \pm 0.06$ Å above the bulk-extrapolated (10$\bar{1}$4) diffraction plane. Similarly, the (0006) position of Se is $P_{0006} \cdot d_{0006} = 0.63 \pm 0.11$ Å above the (0006) diffraction plane. The locus of points marking the intersection of the Se positions in the [10$\bar{1}$4] and the [0001] directions is a line along the [1$\bar{2}$10] direction (i.e. normal to the plane of the page of Fig. 3a). The particular point on this line whose projection in

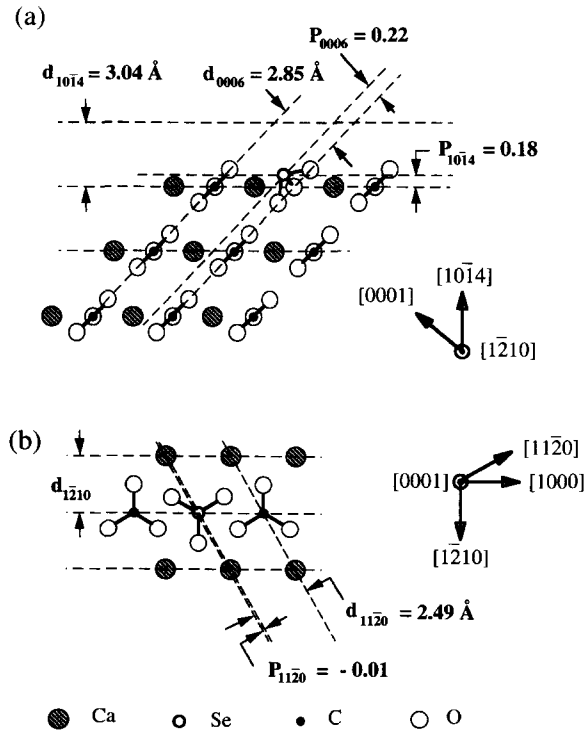

Fig. 3. (a) A schematic depicting the [1$\bar{2}$10] projection of the calcite crystal structure. The (10$\bar{1}$4) and (0006) diffraction planes and measured Se coherent positions (P_H) are indicated as dashed lines. Also included on the top-most (10$\bar{1}$4) layer is a structural model for the SeO_3 adsorbate. (b) A schematic depiction of the [0001] projection of the calcite crystal structure, on which the d-spacing $d_{11\bar{2}0}$ and the measured Se coherent position $P_{11\bar{2}0}$ are indicated.

the [11$\bar{2}$0] direction corresponds to the XSW measured value of $P_{11\bar{2}0} = 0.01 \pm 0.03$ is located within experimental error on the (1$\bar{2}$10) diffraction planes. This is shown in Fig. 3b, where the top view of the calcite (0006) plane is shown. Note that carbon atoms also lie in the (1$\bar{2}$10) plane (i.e. the plane of the page in Fig. 3a).

That the exact site of the Se atom is displaced outward along the [0001] direction from the C site can best be explained if the different geometric shapes of the SeO_3^{2-} ion and the CO_3^{2-} ion are considered. The CO_3^{2-} ion has the shape of a planar equilateral triangle, with C at the center of the triangle. In calcite, the CO_3^{2-} plane defines the (0006) lattice plane. The SeO_3^{2-} ion, on the other hand, has the shape of a low trigonal pyramid, with Se at its apex and O atoms at the corners of its equilateral triangular base.

A plausible model of the local structure of the adsorbed SeO_3^{2-} ion, then, is one where the base of the SeO_3^{2-} pyramid is aligned with the equilateral triangle of the CO_3^{2-} plane. The fact that $P_{10\bar{1}4}$ and P_{0006} are both positive shows that the adsorbed SeO_3^{2-} ions selectively have their Se apices pointing outward from the bulk crystal. This structure is depicted in Fig. 3a. In this model, we assume that the SeO_3^{2-} pyramid has an equilateral triangular base with the Se atom in a central position; this is the geometry observed in most inorganic selenite crystals [19–21]. The height h of the pyramid can be deduced from the present XSW experimental data to test the validity of this structural model. According to the (10$\bar{1}$4) measurement, $h = (0.54 \pm 0.06)/\cos 45.16^\circ = 0.76 \pm 0.09$ Å, where the angle 45.16° is the angle between the (10$\bar{1}$4) and the (0006) planes. Moreover, this agrees within experimental uncertainty with the h value determined from the less precise (0006) XSW data, or $h = 0.63 \pm 0.11$ Å.

Comparisons can be made between these experimentally determined h values for the SeO_3^{2-} pyramid on the calcite surface and those determined by conventional X-ray diffraction in a number of inorganic selenite crystals. In the crystals of most group II cation selenites, h lies primarily within the range between 0.70 and 0.85 Å. A few examples can be cited from the literature: In metal selenites of the form $MSeO_3$, where M denotes Mg, Mn, Co, Ni, Cu or Zn, $h \approx 0.72$ Å [20]. In H_2SeO_3, $h =$ 0.79 Å [22]. In $CaSeO_3 \cdot H_2O$, $h = 0.75$ Å [22]. The agreement between the XSW-measured value of h for this model and these cited values lends additional support to the hypothesis that the triangular oxygen base of the SeO_3^{2-} pyramid lies on the (0006) plane.

The conclusion that SeO_3^{2-} substitutes for CO_3^{2-} at the calcite (10$\bar{1}$4) surface is in agreement with the generally accepted principle that ionic chemisorption on ionic surfaces usually occurs via surface exchange of ions of identical ionicity [7]. Upon adsorption onto the calcite (10$\bar{1}$4) surface, a two-dimensional solid-solution of the chemical form $Ca(SeO_3)_x(CO_3)_{1-x}$ is formed, where $x \approx 0.02$.

The saturation of Se adsorption at 0.02 ML is consistent with the interpretation that this solid-solution only exists in the outermost calcite atomic layer. The absence of adsorbate lattice diffusion and/or epitaxial growth is also characteristic of the Pb^{2+}-adsorbed calcite $(10\bar{1}4)$ surface [11]. X-ray reflectivity experiments confirm that most of the adsorbed Pb only occupies the outermost calcite atomic layers [12]. As with the Pb XSW studies [11], we confirmed with glancing angle X-ray fluorescence and extinction analysis that no significant amount of Se has diffused into the bulk.

The fact that SeO_3^{2-} undergoes chemisorption by calcite has practical implications in the redistribution of trace Se in water. The greater stability of the ionically bonded $Ca(SeO_3)_x(CO_3)_{1-x}$ phase implies that SeO_3^{2-} ions are preferentially removed from water by calcite. However, the absence of either lattice diffusion towards the crystal bulk or epitaxial growth limits Se uptake. This limit should be comparable to the measured adsorption coverage of $\Theta = 0.02$ ML, or 10^{13} atoms cm^{-2}. With the recent availability of synchrotron X-ray beamlines with much higher-intensities, one could perform a rapid succession of in situ XSW measurements to determine adsorption rate constants.

The X-ray standing wave method was used to investigate the adsorption from an aqueous solution of the two common Se oxyanions, selenite and selenate, on the calcite $(10\bar{1}4)$ cleavage surface. The selenite ions adsorbed with a coverage of 0.02 equivalent monolayers, whereas adsorption of the selenate ion was inhibited. Triangulation by XSW of the Se position for adsorbed selenite, using the calcite $(10\bar{1}4)$, (0006) and $(11\bar{2}0)$ reflections showed that SeO_3^{2-} groups substituted for surface CO_3^{2-} groups via ion exchange to form a two-dimensional solid-solution of $Ca(SeO_3)_{0.02}(CO_3)_{0.98}$. The high coherent fraction of the Se revealed by the XSW measurements shows that the selenite pyramids have a strongly preferred orientation.

Acknowledgements

This research was supported by the Geoscience and Materials Science Research Programs of the Office of Basic Energy Sciences, U.S. Department of Energy, under contract W-31-109-Eng-38 to Argonne National Laboratory and DOE contract DE-AC02-76CH00016 to the National Synchrotron Light Source at Brookhaven National Laboratory, and by the National Science Foundation under contract DMR-9632472 to the Materials Research Center at Northwestern University.

References

[1] R.J. Reeder, G.M. Lamble, J.-F. Lee, W.J. Staudt, Geochim. Cosmochim. Acta 58 (1994) 5639.
[2] S. Sharma, R. Singh, CRC Crit. Rev. Environ. Control 13 (1983) 23.
[3] J.H. Howard, Geochim. Cosmochim. Acta 41 (1977) 1665.
[4] J.C. Ryden, J.K. Syers, R.W. Tillman, J. Soil Sci. 38 (1987) 211.
[5] K.F. Hayes, A.L. Roe, G.E. Brown, K.O. Hodgson, J. O Leckie, G.A. Parks, Science 238 (1987) 783.
[6] A. Manceau, L. Charlet, J. Colloid. Interface Sci. 168 (1994) 87.
[7] J.M. Zachara, C.E. Cowan, C.T. Resch, Geochim. Cosmochim. Acta 55 (1991) 1549.
[8] C.E. Cowan, J.M. Zachara, C.T. Resch, Geochim. Cosmochim. Acta 54 (1990) 2223.
[9] W.J. Staudt, R.J. Reeder, M.A.A. Schoonen, Geochim. Cosmochim. Acta 58 (1994) 2087;
G.M. Lamble, J.F. Lee, W.J. Staudt, R.J. Reeder, Physica B 208/209 (1995) 589.
[10] J.A. Golovchenko, J.R. Patel, D.R. Kaplan, P.L. Cowan, M.J. Bedzyk, Phys. Rev. Lett. 49 (1982) 560.
[11] Y. Qian, N.C. Sturchio, R.P. Chiarello, P.F. Lyman, T.-L. Lee, M.J. Bedzyk, Science 265 (1994) 1555.
[12] N.C. Sturchio, R.P. Chiarello, L. Cheng, P.F. Lyman, M.J. Bedzyk, Y. Qian, H. You, D. Yee, P. Geissbuhler, L.B. Sorensen, Y. Liang, D. Baer, Geochim. Cosmochim. Acta (1997) 61.
[13] B.W. Batterman, H. Cole, Rev. Mod. Phys. 36 (1964) 681.
[14] J. Zegenhagen, Surf. Sci. Rep. 18 (1993) 199.
[15] P.F. Lyman, Y. Qian, M.J. Bedzyk, Surf. Sci. 325 (1995) L385.
[16] F. Ohnesorge, G. Binnig, Science 260 (1993) 1451.
[17] Y. Liang, A.S. Lea, D.R. Baer, M.H. Engelhard, Surf. Sci. 351 (1996) 172.
[18] R.P. Chiarello, N.C. Sturchio, Geochim. Cosmochim. Acta 59 (1995) 4557.
[19] P.R. Weiss, J.-P. Wendling, D. Grandjean, Acta Cryst. 20 (1966) 563.
[20] K. Kohn, K. Inoue, O. Horie, S. Akimoto, J. Solid State Chem. 18 (1976) 27.
[21] J. Valkonen, T. Losoi, Acta Cryst. C41 (1985) 652.
[22] R.W.G. Wyckoff, Crystal Structures, Wiley, New York, 1964.